Supplementary Information

Sascha Feldmann[1†], Stuart Macpherson[1†], Satyaprasad P. Senanayak[1], Mojtaba Abdi-Jalebi[1], Jasmine P.H. Rivett[1], Guangjun Nan[2], Gregory D. Tainter[1], Tiarnan A. S. Doherty[1], Kyle Frohna[1], Emilie Ringe[3,4], Richard H. Friend[1], Henning Sirringhaus[1], Michael Saliba[5], David Beljonne[6], Samuel D. Stranks[1*], and Felix Deschler[1,7*]

[1]Cavendish Laboratory, University of Cambridge, Cambridge, UK

[2]Department of Physics, Zhejiang Normal University, Jinhua 321004, China

[3]Department of Materials Science and Metallurgy, University of Cambridge, Cambridge, UK

[4]Department of Earth Sciences, University of Cambridge, Cambridge, UK

[5]Adolphe Merkle Institute, University of Fribourg, CH-1700 Fribourg, Switzerland

[6]Chimie des Matériaux Nouveaux, Université de Mons, B-7000 Mons, Belgium

[7]Walter Schottky Institut and Physik Department, Technische Universität München, Garching, Germany

[†]these authors contributed equally to this work

*e-mail: sds65@cam.ac.uk, felix.deschler@wsi.tum.de

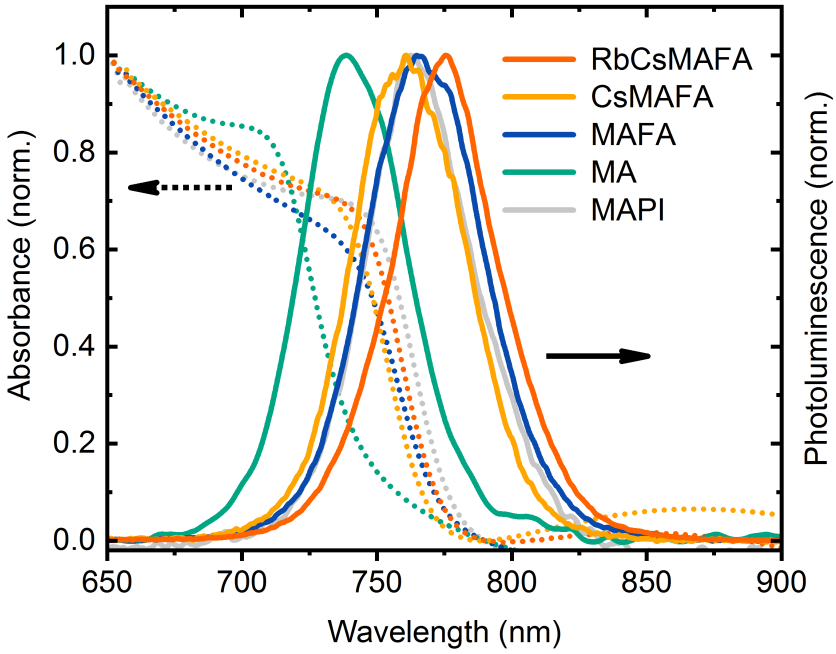

Supporting Figure 1: Absorbance (dotted) and photoluminescence (solid) spectra of the various perovskite compositions examined in this study.

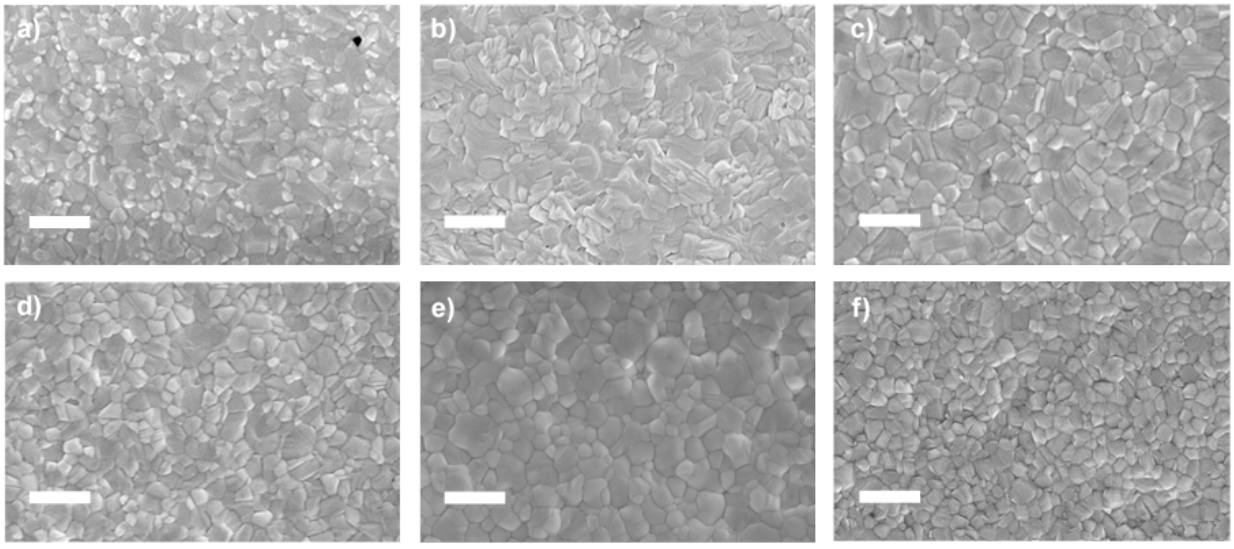

Supporting Figure 2: Scanning electron microscopy (SEM) images of **(a)** MA-I, **(b)** MA, **(c)** MAFA, **(d)** CsMAFA, **(e)** RbCsMAFA and **(f)** KCsMAFA samples. Scale bar is 1 μm.

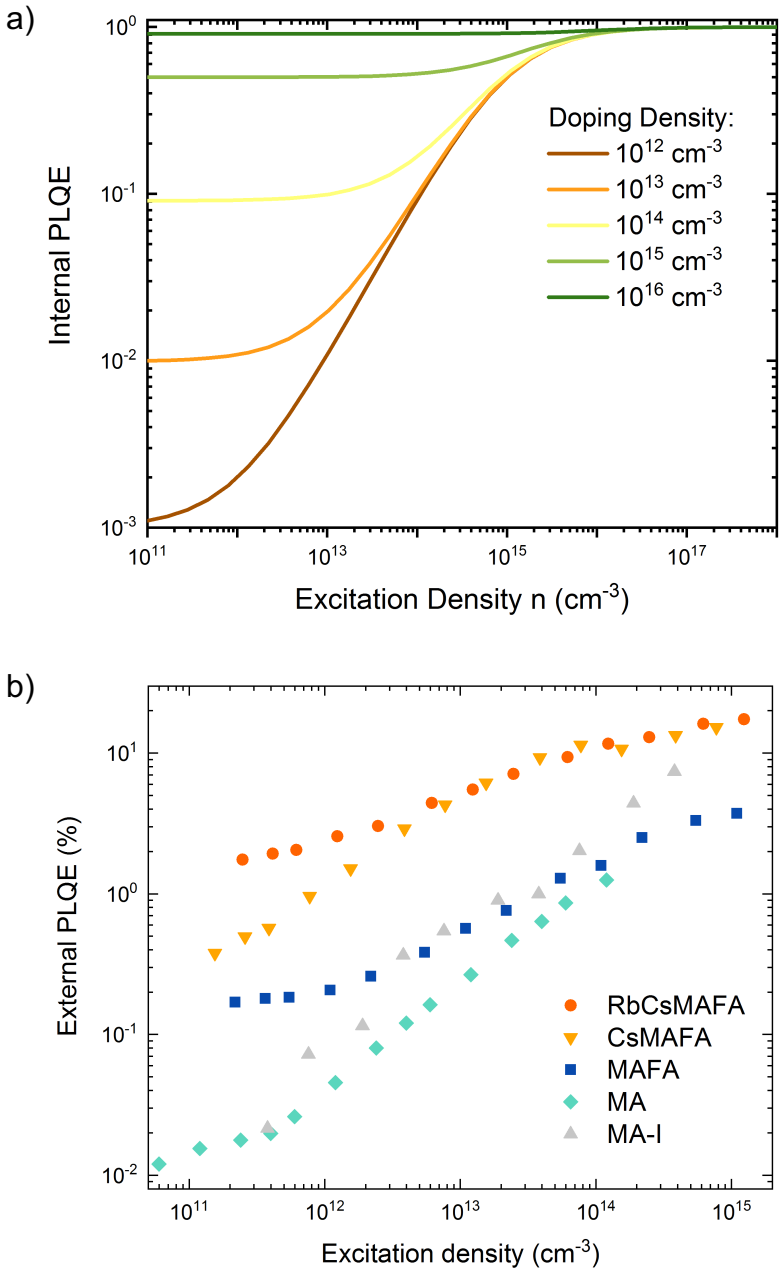

Supporting Figure 3: (a) Influence of doping carrier density (N_D) on fluence-dependent photoluminescence quantum efficiency (PLQE) behavior, as described by the rate equation model in the main text. High doping densities lead to an increased base level PLQE. **(b)** Measured PLQE dependence on excited carrier density. Variation with excitation density is in accordance with the modelled behaviour, with PLQE values levelling out at low carrier density. Samples with higher doping carrier density exhibit higher base level PLQE.

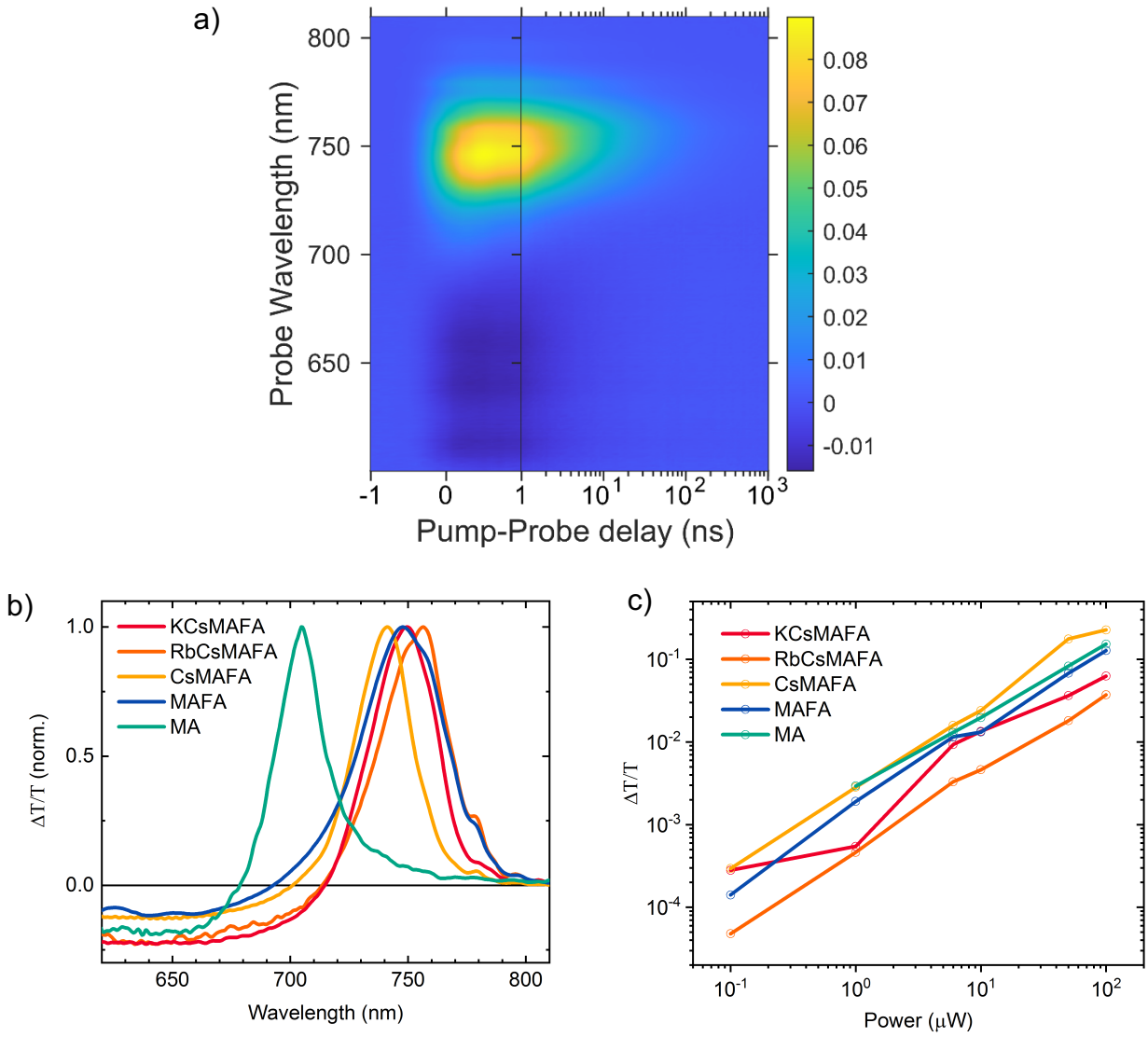

Supporting Figure 4: (a) Typical 2D map of transient absorption (TA) spectroscopy data, for a KCsMAFA sample. The color scale shows the fractional change in sample transmission. The ground state bleach is observed as a positive feature, centered around 750 nm. A photoinduced absorption feature is present at higher energy. **(b)** Normalized TA spectra at 1 ns pump-probe delay. The addition of the large FA^+ cation narrows the band gap causing a red shift in the ground state bleach of the mixed cation samples. Small dopant concentrations of CsI, RbI and KI have little effect on the band gap thereafter. **(c)** Initial ground state bleach intensity scaling linearly with pump power. This relationship provides the conversion from bleach intensity to carrier density.

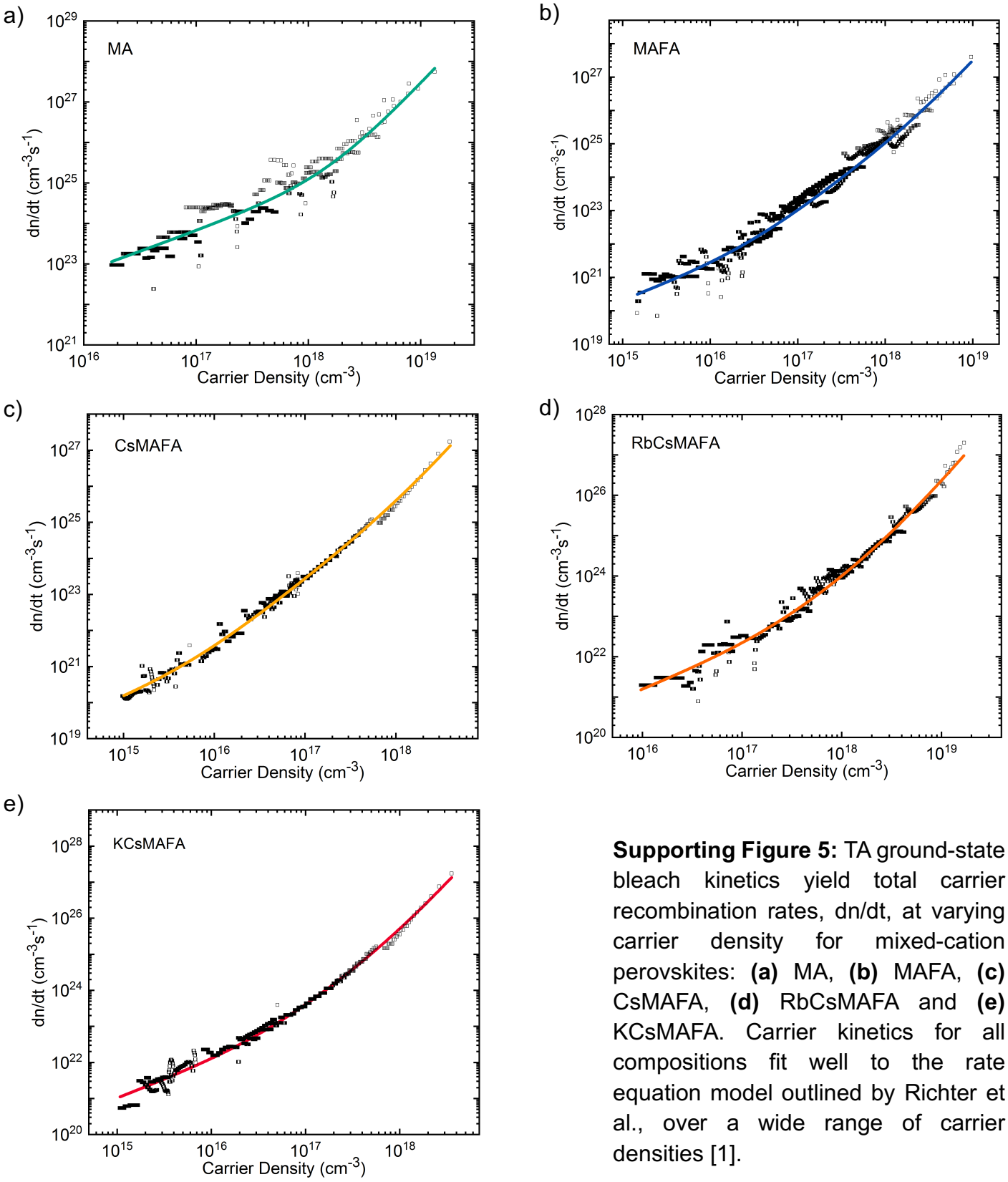

Supporting Figure 5: TA ground-state bleach kinetics yield total carrier recombination rates, dn/dt, at varying carrier density for mixed-cation perovskites: **(a)** MA, **(b)** MAFA, **(c)** CsMAFA, **(d)** RbCsMAFA and **(e)** KCsMAFA. Carrier kinetics for all compositions fit well to the rate equation model outlined by Richter et al., over a wide range of carrier densities [1].

	a (s^{-1})	b (cm^3s^{-1})	c (cm^6s^{-1})	a^* (s^{-1}) PL
MA-I	$2.4x10^{6}$	$1.3x10^{-11}$	$5.7x10^{-30}$	$< 9.8x10^{6}$
MA	$(6.38\pm0.20)x10^{6}$	$(3.17\pm0.61)x10^{-12}$	$(2.08\pm0.26)x10^{-30}$	$3.1x10^{7}$
MAFA	$(1.98\pm0.07)x10^{5}$	$(7.27\pm0.26)x10^{-12}$	$(1.93\pm0.23)x10^{-30}$	$< 3.4x10^{6}$
CsMAFA	$(3.46\pm0.17)x10^{5}$	$(5.29\pm0.30)x10^{-12}$	$(4.99\pm2.16)x10^{-31}$	$< 4.8x10^{6}$
RbCsMAFA	$(1.50\pm0.04)x10^{5}$	$(6.27\pm0.37)x10^{-13}$	$(1.30\pm0.64)x10^{-31}$	$< 3.0x10^{6}$
KCsMAFA	$(6.78\pm0.20)x10^{5}$	$(1.41\pm0.14)x10^{-12}$	$(2.06\pm1.35)x10^{-31}$	$2.3x10^{6}$

Supporting Table 1: Rate constants (*a, b, c)* extracted from the fitted curves of figure S5. MA-I parameters provided as a reference. Films containing FA have reduced rate constants owing to their longer lifetimes. Monomolecular PL rate constants (*a**) were extracted via a mono-exponential fit of PL kinetics, excluding the initial intensity drop in mixed halide containing samples showing it.

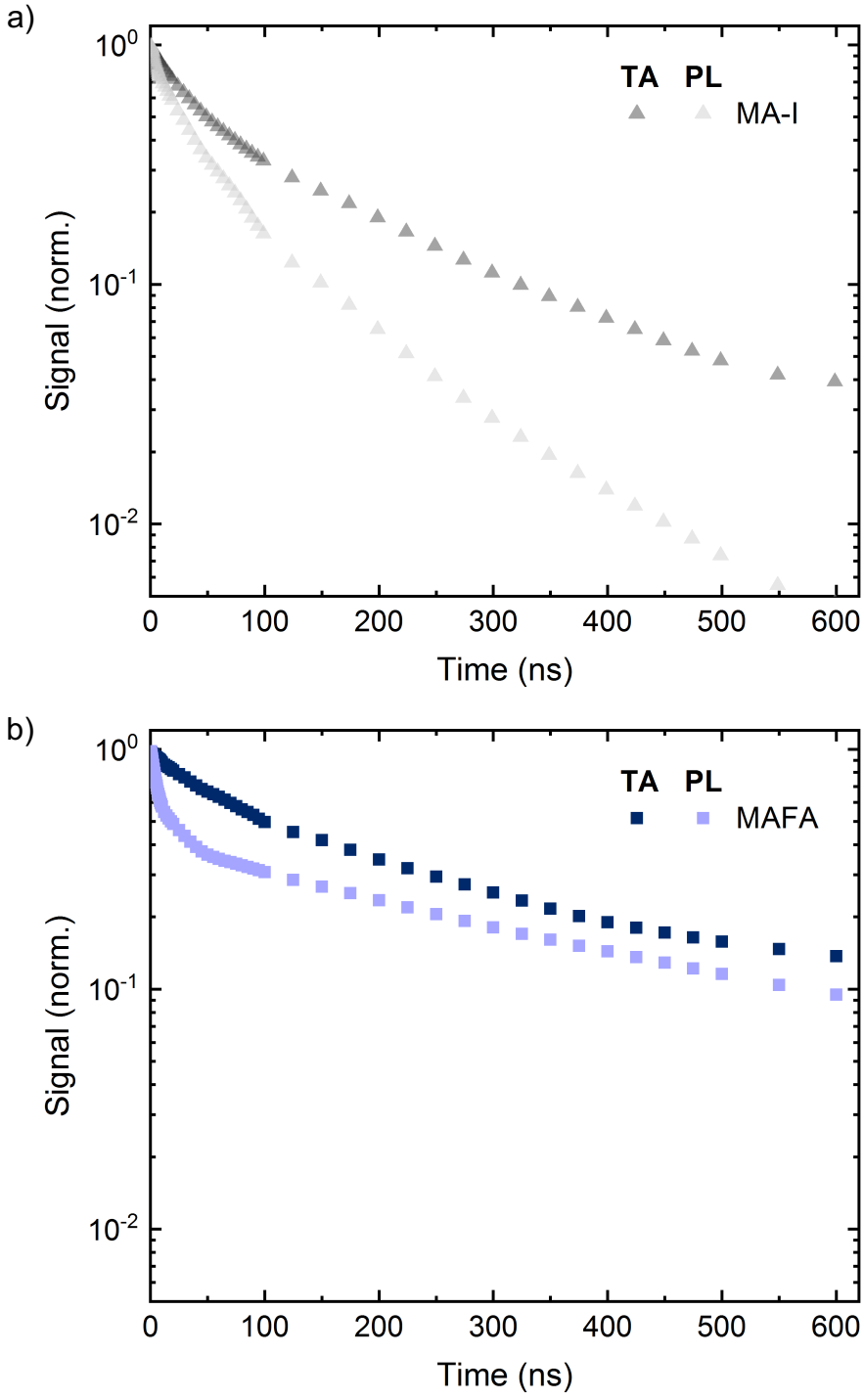

Supporting Figure 6: Normalized Transient Absorption (TA) and Photoluminescence (PL) kinetics of **(a)** MA-I and **(b)** MAFA. In MA-I, PL is a bimolecular process and therefore the signal decays rapidly relative to the TA which is dominated by first-order processes. In MAFA, the PL signal experiences an initial drop indicating a reduction in radiative recombination rate, before plateauing and tracking with the mono-molecular TA decay. This is characteristic of the PL displaying first-order radiative recombination. For all curves, carrier density at time zero, $n_0 = 10^{16}$ cm^{-3}.

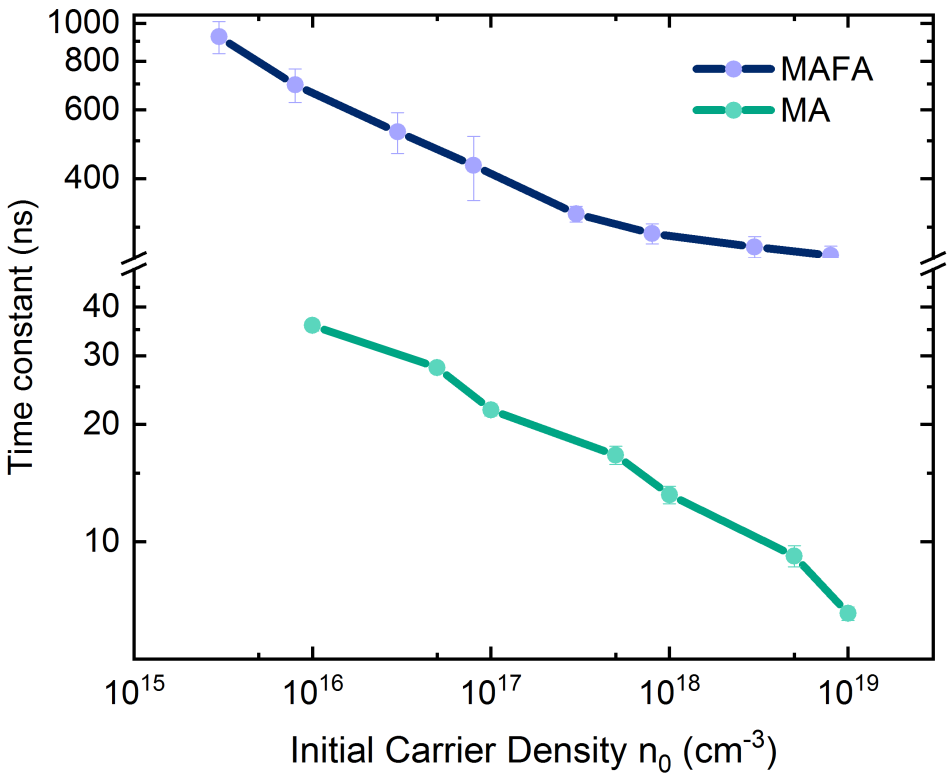

Supporting Figure 7: Photoluminescence time constants as a function of initial carrier density (n_0), for MA and MAFA samples, extracted via a monoexponential fit. In MAFA, the radiative lifetime increases rapidly at low carrier density and remains high even at the largest n_0.

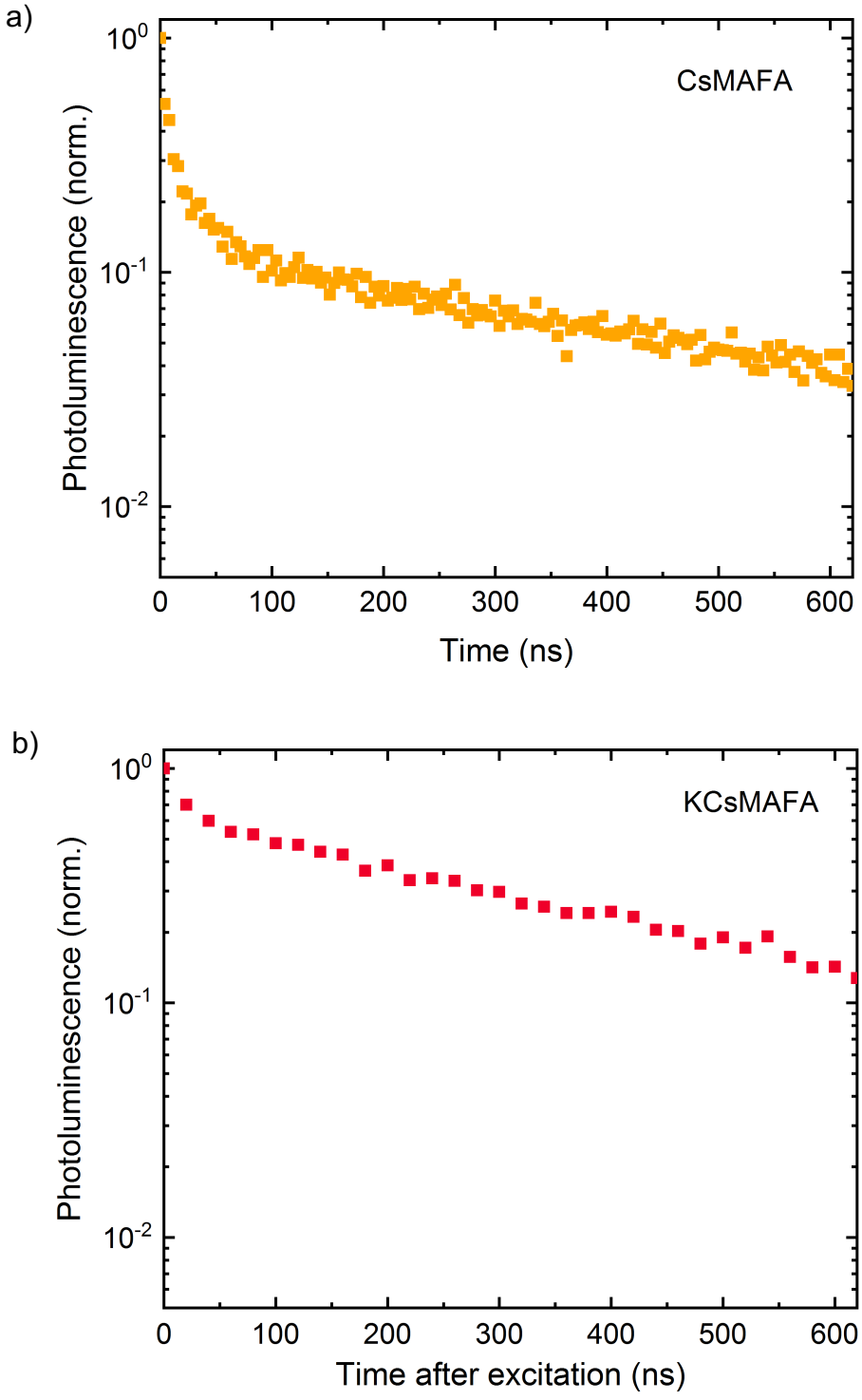

Supporting Figure 8: Normalized Photoluminescence kinetics of **(a)** CsMAFA and **(b)** KCsMAFA. Both compositions show an initial drop in PL intensity, since they are mixed-halide-based. Initial carrier density at time zero , $n_0 = 10^{16}$ cm^{-3}.

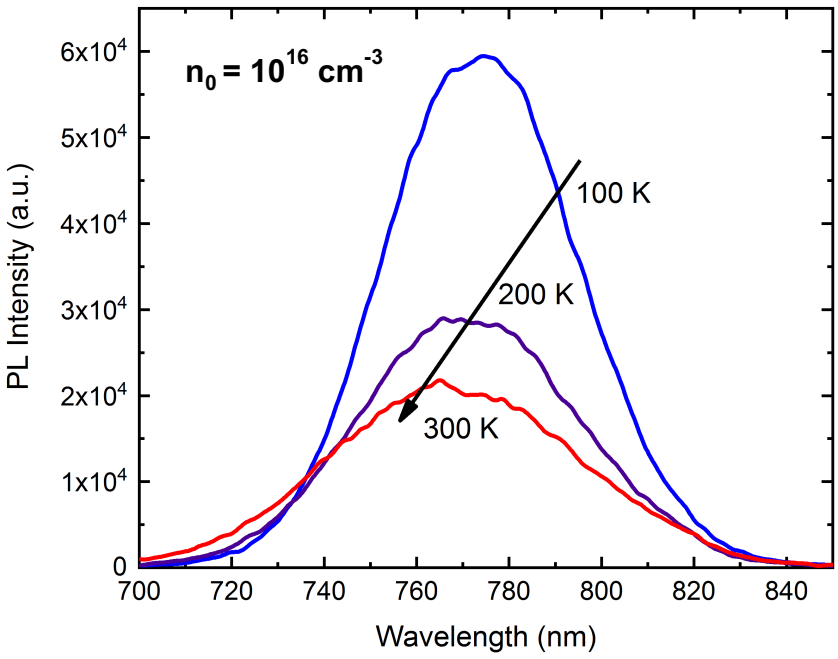

Supporting Figure 9: Temperature dependence of PL spectra of MAFA, with an initial carrier density of 10^{16} cm^{-3}. Excitation was provided by a 400 nm laser pulse (1 kHz repetition rate, 90 fs pulse length). As temperature increases, absolute PL decreases (as observed in MA-I) but high energy emission is activated due to the extra thermal energy of carriers.

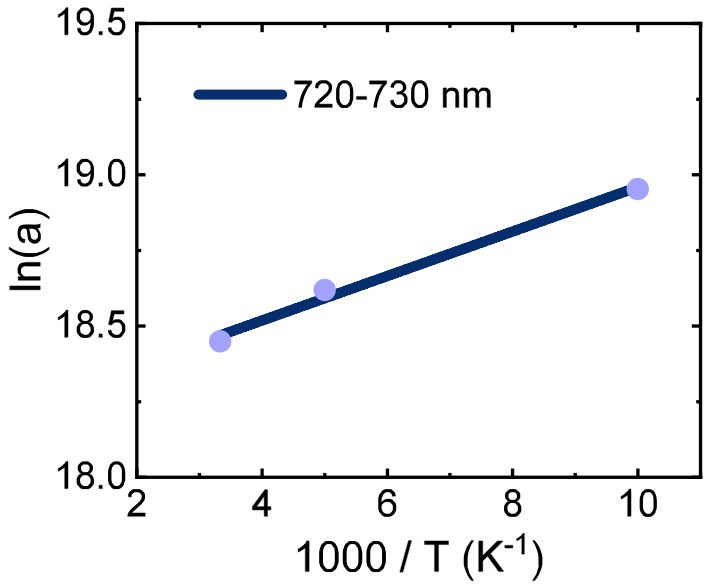

Supporting Figure 10: Arrhenius-like plot of high energy kinetics from figure 2(a), where *a* is the rate constant of the PL decay at sample temperature, *T*. The slope yields a deactivation energy of (31 ± 3) meV, for carrier localization.

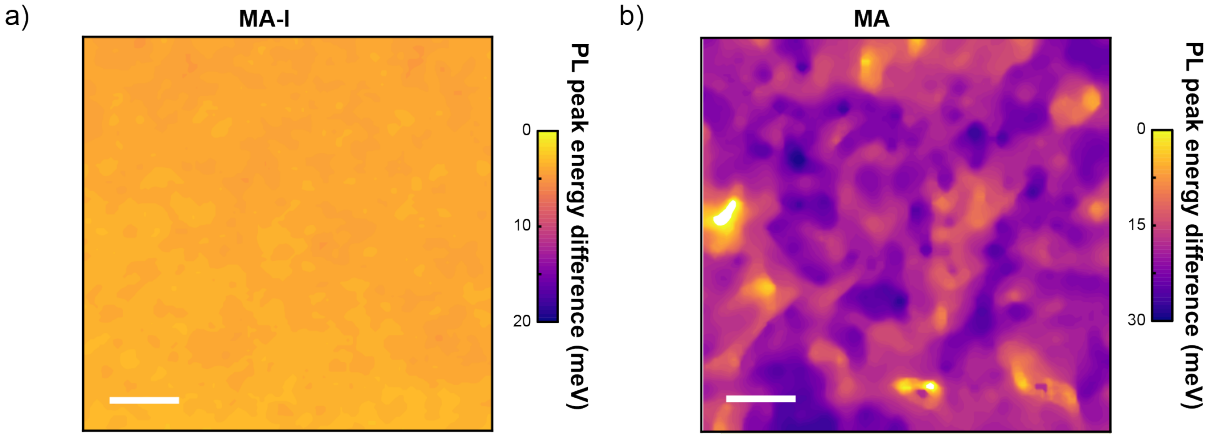

Supporting Figure 11: Confocal Microscopy PL maps of **(a)** MA-I and **(b)** MA films, showing contrasting degrees of energy heterogeneity. MA-I has an extremely uniform PL peak energy owing to the pure iodide anion. As with MAFA, the MA film displays energy non-uniformity on the micron-scale with variations of ~30 meV in PL peak energy. Scalebar is 5 μm.

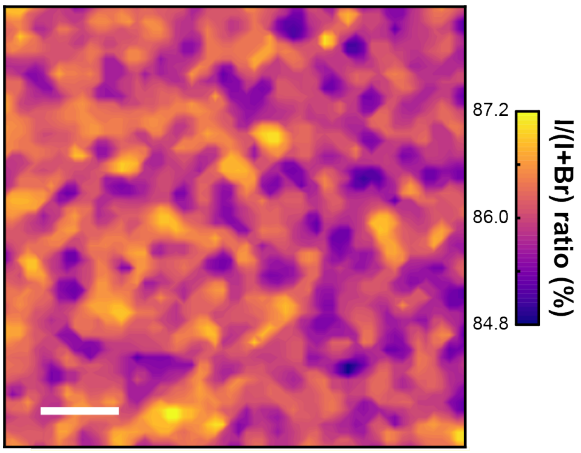

Supporting Figure 12: Electron probe microanalyzer (EPMA) data for a CsMAFA sample, mapping the ratio of iodine L_α emission to total halide emission (iodine L_α + bromine L_α). Significant compositional heterogeneity is observed along with evidence of iodine-rich regions. Scalebar is 5 μm.

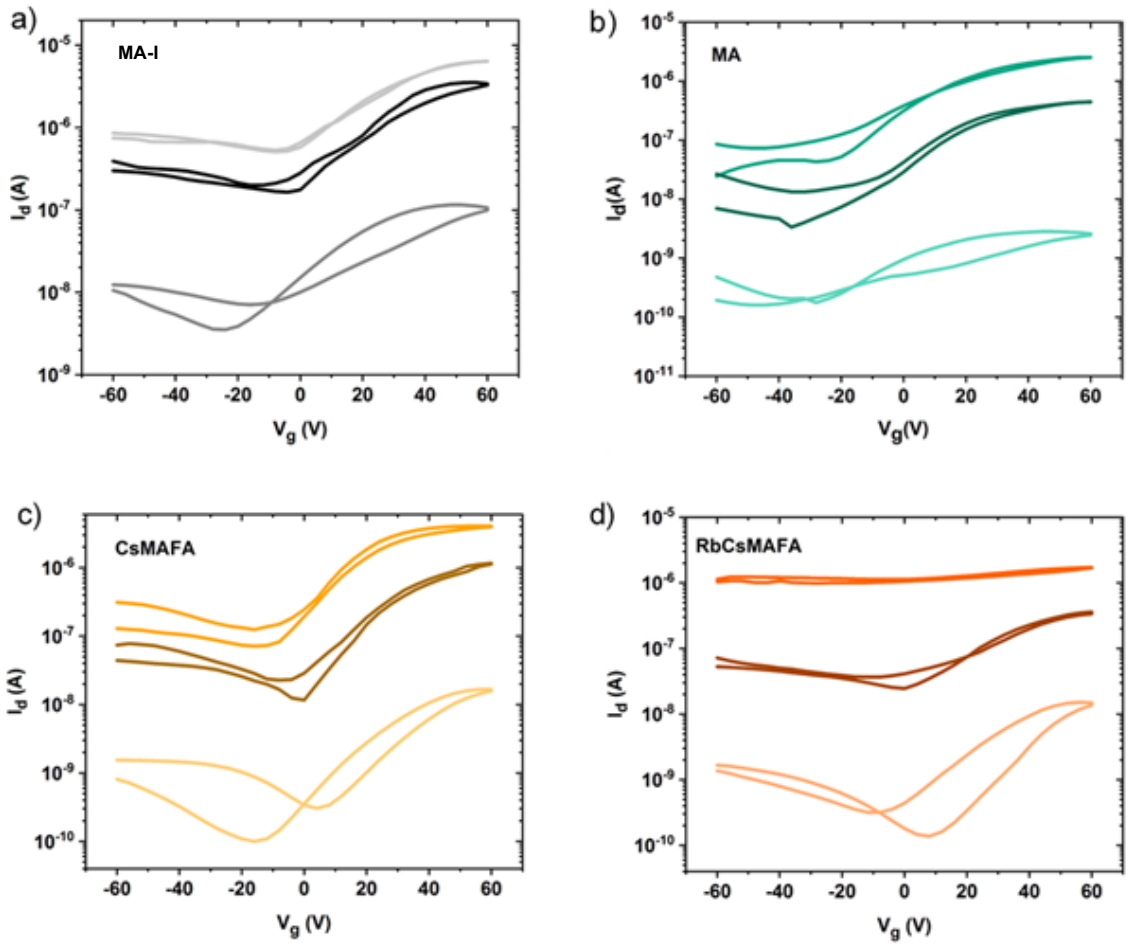

Supporting Figure 13: Transfer characteristics of bottom gate, bottom contact thin-film field-effect transistors with perovskite layers of **(a)** MA-I, **(b)** MA, **(c)** CsMAFA and **(d)** RbCsMAFA under three levels of photoexcitation (dark, 0.05 sun and 0.5 sun, respectively). Drain voltage (V_d) fixed at 60 V, measurements carried out at temperature of 300 K.

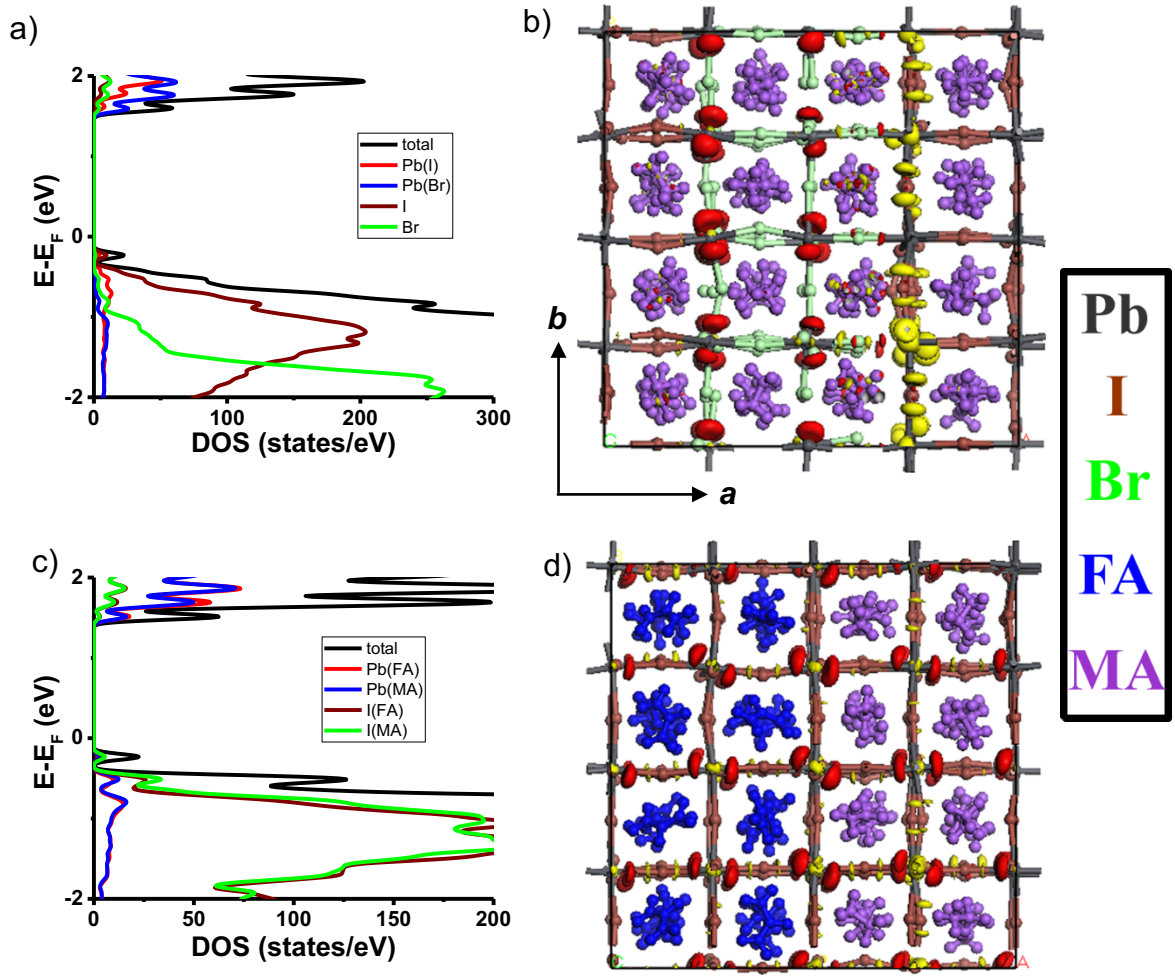

Supporting Figure 14: (a) DOS and **(b)** Charge densities of the lowest excited state for the optimized ground-state geometry of $MAPbI_{1.5}Br_{1.5}$ with $MAPbI_3/MAPbBr_3$ heterojunction. **(c)** and **(d)**: No intrinsic driving force for charge segregation across the MA–FA interface. **(c)** DOS and **(d)** Charge densities of the lowest excited state for the optimized ground-state of $FA_{0.5}MA_{0.5}PbI_3$ with $FAPbI_3/MAPbI_3$ heterojunction along *a* axis. The electron (hole) density is shown in red (yellow) in (b) and (d). The value of the isosurface is 1.5×10^{-3} e/Å^3 in (b) and 7.0×10^{-4} e/Å^3 in (d).

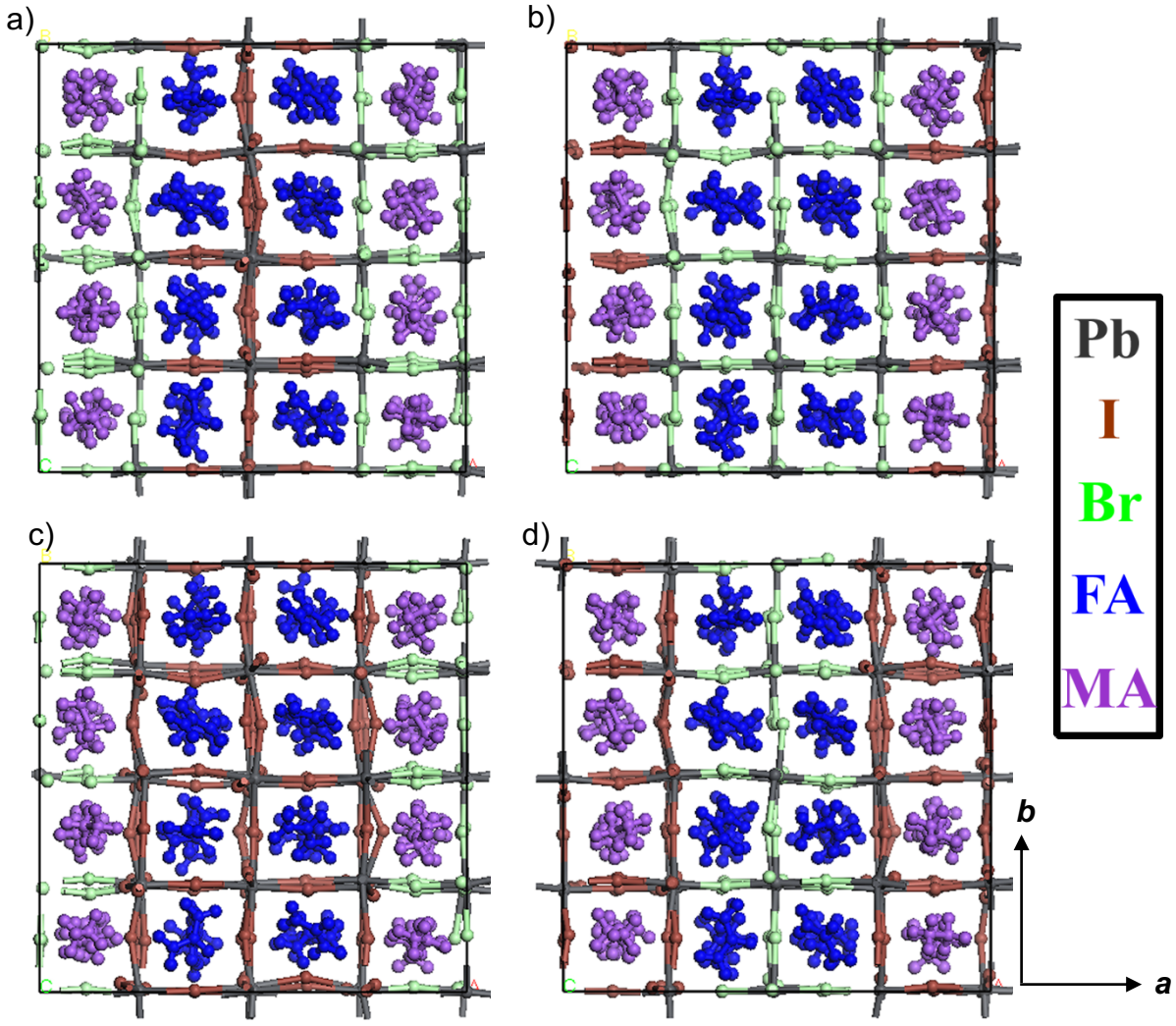

Supporting Figure 15: (a) $MAPbBr_3/FAPbI_3$ heterojunction with I:Br = 1:2; **(b)** $MAPbI_3/FAPbBr_3$ heterojunction with I:Br = 1:2; **(c)** $MAPbBr_3/FAPbI_3$ heterojunction with I:Br = 2:1; **(d)** $MAPbI_3/FAPbBr_3$ heterojunction with I:Br = 2:1. The ground-state energy for the heterojunction in (a) is 28.3 meV/nm^3 smaller than the ground-state energy for the heterojunction in (b). The ground-state energy for the heterojunction in (c) is 90.9 meV/nm^3 smaller than the ground-state energy for the heterojunction in (d). These results indicate that the bulky FA cations fit more easily into the cavity around the large iodide ions, which might be ascribed to the reduced rigidity in the Pb-I cages compared with Pb-Br.

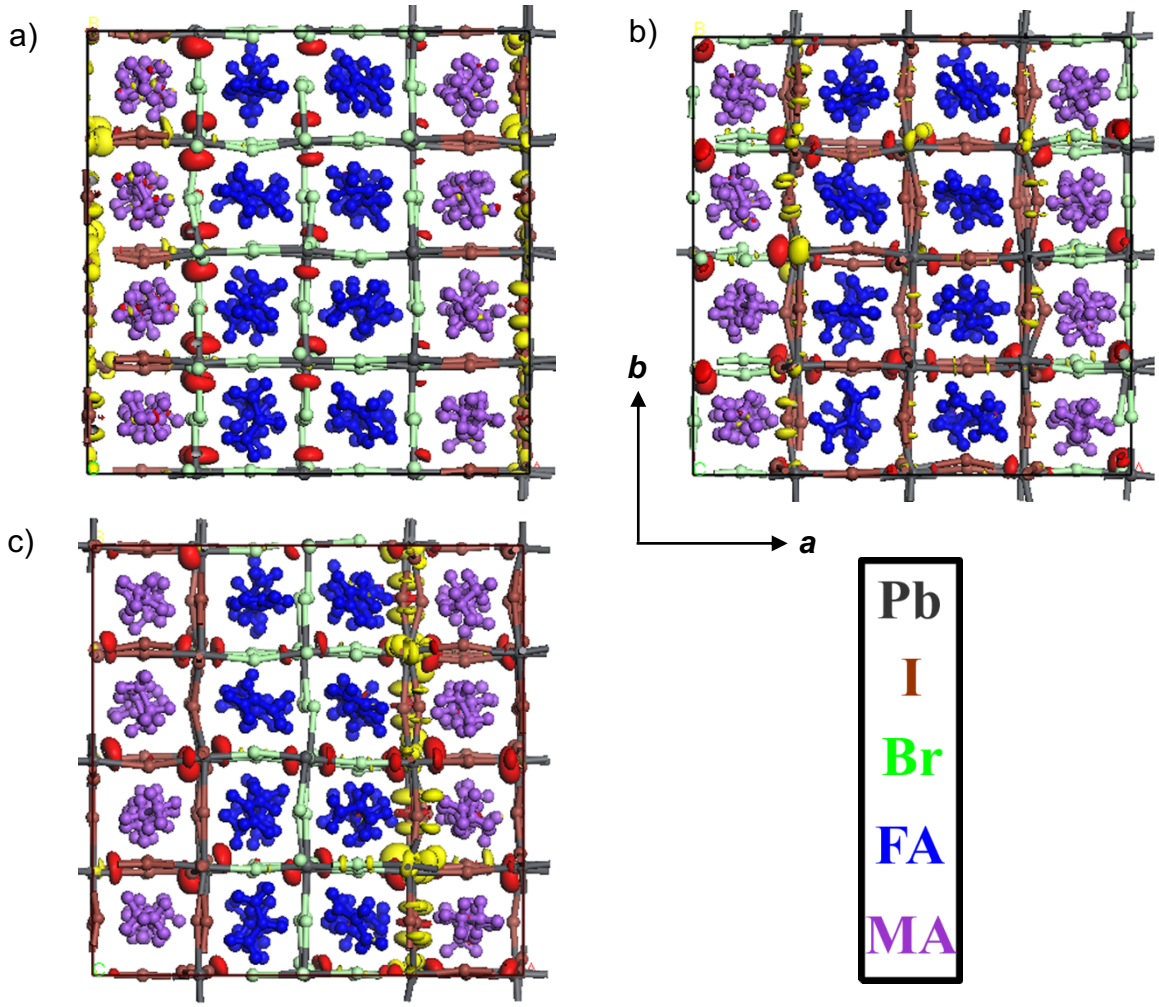

Supporting Figure 16: Charge densities of the lowest excited state for the optimized ground-state geometries of $MAPbI_3/FAPbBr_3$ and $MAPbBr_3/FAPbI_3$ heterojunctions. **(a)** $MAPbI_3/FAPbBr_3$ heterojunction with I:Br = 1:2; **(b)** $MAPbBr_3/FAPbI_3$ heterojunction with I:Br = 2:1; **(c)** $MAPbI_3/FAPbBr_3$ heterojunction with I:Br = 2:1. The electron (hole) density is shown in red (yellow). The value of isosurface is 1.5×10^{-3} e/Å^3 in (a) and 1.0×10^{-3} e/Å^3 in (b) and (c).

References

[1] Richter, J. M. et al. Enhancing photoluminescence yields in lead halide perovskites by photon recycling and light out-coupling. *Nat. Commun*. **7**, 13941 (2016).